8-1-2003

Representation Of A Nonspherical Ice Particle By A Collection Of Independent Spheres For Scattering And Absorption Of Radiation: 2. Hexagonal Columns And Plates

Steven P. Neshyba
University of Puget Sound, nesh@pugetsound.edu

Thomas C. Grenfell
Department of Atmospheric Sciences, University of Washington, Seattle, Washington, USA

Stephen G. Warren
Department of Atmospheric Sciences, University of Washington, Seattle, Washington, USA

Citation

Neshyba, Steven P., Tc Grenfell, and Sg Warren. 2003. "Representation of a nonspherical ice particle by a collection of independent spheres for scattering and absorption of radiation: 2. Hexagonal columns and plates." Journal Of Geophysical Research-atmospheres 108(D15): 4448-4448.

Representation of a nonspherical ice particle by a collection of independent spheres for scattering and absorption of radiation: 2. Hexagonal columns and plates

Steven P Neshyba
Department of Chemistry, University of Puget Sound, Tacoma, Washington, USA

Thomas C. Grenfell and Stephen G. Warren
Department of Atmospheric Sciences, University of Washington, Seattle, Washington, USA

Received 4 December 2002; revised 24 April 2003; accepted 13 May 2003; published 5 August 2003.

[1] A cloud of nonspherical ice particles may be represented in radiation models by a collection of spheres, in which the model cloud contains the same total volume of ice and the same total surface area as the real cloud but not the same number of particles. The spheres then have the same volume-to-area (V/A) ratio as the nonspherical particle. In previous work this approach was shown to work well to represent randomly oriented infinitely long circular cylinders for computation of hemispherical reflectance, transmittance, and absorptance. In this paper the results have been extended to hexagonal columns and plates using a geometric optics technique for large particles and finite-difference-time-domain theory (FDTD) for small particles. The extinction efficiency and single-scattering coalbedo for these prisms are closely approximated by the values for equal-V/A spheres across the ultraviolet, visible, and infrared from 0.2 to 25 μm wavelength. Errors in the asymmetry factor can be significant where ice absorptance is weak, at visible wavelengths for example. These errors are greatest for prisms with aspect ratios close to 1. Errors in hemispheric reflectance, absorptance, and transmittance are calculated for horizontally homogeneous clouds with ice water paths from 0.4 to 200,000 g m^{-2} and crystal thicknesses of 1 to 400 μm, to cover the range of crystal sizes and optical depths from polar stratospheric clouds (PSCs) through cirrus clouds to surface snow. The errors are less than 0.05 over most of these ranges at all wavelengths but can be larger at visible wavelengths because of the ideal shapes of the prisms. The method was not tested for, and is not expected to be accurate for, angle-dependent radiances. *INDEX TERMS:* 0320 Atmospheric Composition and Structure: Cloud physics and chemistry; 0360 Atmospheric Composition and Structure: Transmission and scattering of radiation; 1863 Hydrology: Snow and ice (1827); 3359 Meteorology and Atmospheric Dynamics: Radiative processes; 5464 Planetology: Solid Surface Planets: Remote sensing; *KEYWORDS:* ice, scattering, equivalent spheres

Citation: Neshyba, S. P, T. C. Grenfell, and S. G. Warren, Representation of a nonspherical ice particle by a collection of independent spheres for scattering and absorption of radiation: 2. Hexagonal columns and plates, *J. Geophys. Res.*, *108*(D15), 4448, doi:10.1029/2002JD003302, 2003.

1. Introduction

[2] Models to calculate absorption and scattering of light by ice crystals in clouds and snow commonly represent the crystals by "equivalent spheres." This approach allows the use of Mie theory for the single-scattering computations, which reduces the computation time considerably. Furthermore, a great variety of particle shapes occur in ice clouds, and in many cases the exact shapes are unknown, so to represent these clouds in climate models it is appropriate to use simpler parameterizations. It is also often convenient, in the analysis of crystals collected in aircraft experiments in clouds, to summarize the size and shape distribution by a single "effective radius." Remote-sensing methods also often obtain a single effective radius, raising the question of how this number relates to the assortment of crystals in the cloud and how to use the remotely sensed effective radii in cloud modeling. Equivalent-sphere models provide a link between the highly simplified representations that arise in remote-sensing and climate-modeling contexts and the detailed representations that arise in in situ measurement and computational contexts.

[3] Three choices of equivalent spheres have been used [*Grenfell and Warren*, 1999, Figure 2]. A nonspherical particle may be represented by a sphere of the same volume, *V*, or by a sphere of the same surface area, *A*, or by a collection of spheres with the same volume-to-

0148-0227/03/2002JD003302

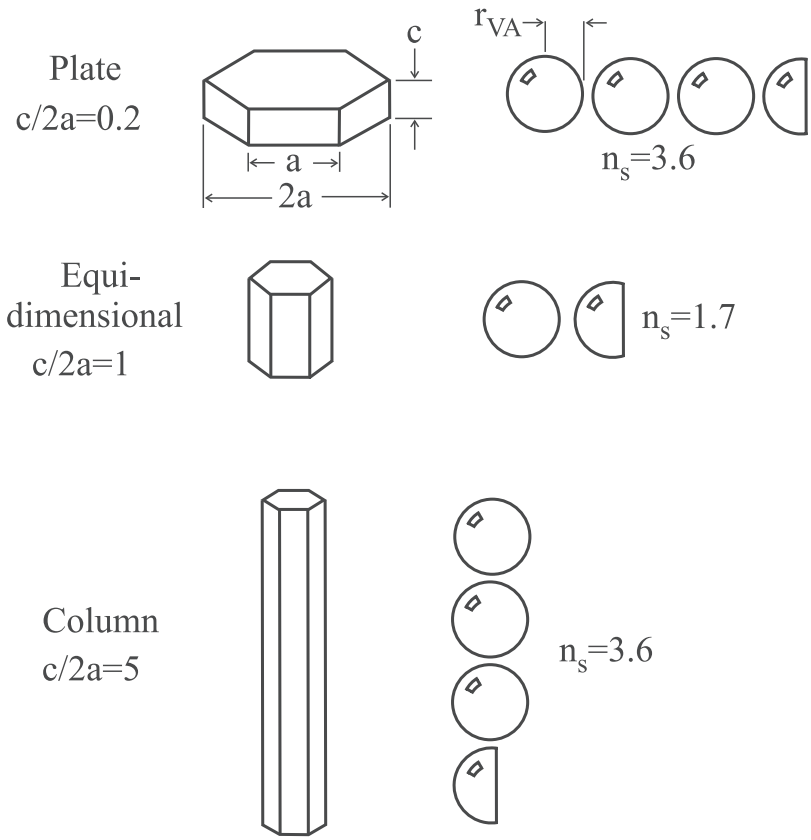

Figure 1. Equal-*V/A* spheres corresponding to hexagonal prisms for aspect ratios ($\Gamma = c/2a$) of 0.2, 1, and 5. All three of these prisms have the same volume-to-area ratio, so the radius of the equivalent spheres is the same for each. The particles are drawn to scale.

surface-area ratio, *V/A*. For equal-volume and equal-area equivalent spheres, the number of particles in the model cloud, n_s, is the same as in the real cloud, n, but for equal-*V/A* spheres, $n_s > n$ (Figures 1 and 2). The model cloud can conserve any two of the three properties of the real cloud: total volume of ice, total surface area of particles, and number of particles. *Fu* [1996] and *Fu et al.* [1998] showed for some specific cases that the equal-*V/A* prescription was superior to the other two representations. For weakly absorbing particles the absorption is proportional to the volume, but the scattering is proportional to the surface area. It is thus important that the model cloud have the correct area and the correct volume (or mass) of ice. Matching the number of particles is apparently much less important. In fact, a particular advantage of the equal-*V/A* representation is that it can be applied unambiguously to a collection of particles in a terrestrial snowpack, for example, where the identity of the individual snow particles is not always well defined.

[4] In the predecessor to this paper, *Grenfell and Warren* [1999, hereinafter referred to as GW99] reviewed the use of the volume-to-area ratio for both cloud optics and snow optics and examined the accuracy of the equal-*V/A* prescription, surveying the entire wavelength domain 0.2 to 50 μm over the entire range of ice crystal radii and ice-water paths from polar stratospheric clouds to surface snow (1–500 μm; 0.4 to 200,000 g m^{-2}). To cover the entire range of wavelengths and sizes, they chose as their nonspherical shape

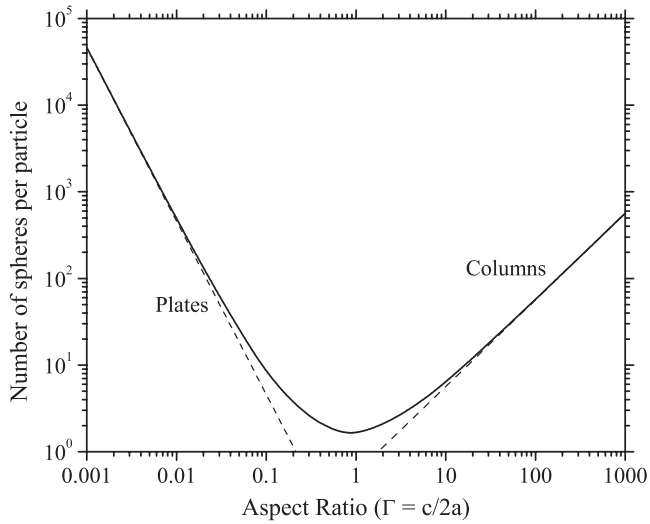

Figure 2. Number of equal-*V/A* spheres per prism as a function of aspect ratio. The dashed lines show results of the asymptotic formulae for thin plates (equation (8b)) and long columns (equation (7b)). The minimum number of spheres per particle is 1.65 for $\Gamma = 0.866$.

randomly oriented, infinitely long circular cylinders because an exact solution is available for all size parameters.

[5] The equal-*V/A* spheres did an excellent job of mimicking the angular averaged single-scattering and multiple-scattering properties of clouds of circular cylinders across the entire wavelength domain and for all cylinder radii and cloud thicknesses. The errors in hemispheric reflectance and absorptance were generally 0 to 0.02 and rarely exceeded 0.05. Because of that success, we have now conducted a similarly comprehensive survey to test the ability of spheres to represent some ice crystal shapes that do exist in real clouds: hexagonal columns and plates (e.g., Figure 1 of GW99).

[6] Hemispheric fluxes are less sensitive to particle shape than are radiances because radiances are affected by details of the phase function whereas fluxes are sensitive only to the low-order moments of the phase function. Phase functions of nonspherical particles may differ dramatically from those of spheres and yet have the same asymmetry parameter (e.g., Figure 5 of GW99). We provide comparisons only for angularly averaged quantities such as hemispheric reflectance and transmittance and the single-scattering quantities required to compute them. So, for example, we compare the asymmetry parameters but not the details of the phase matrix. We are thus testing the accuracy of the equivalent-sphere formulation for use in energy budget studies, not for remote sensing; however, we do make some qualitative comments about the relevance of the formulation for remote sensing.

[7] The error survey in this paper differs in two ways from that of GW99. There is an additional variable, the length-to-width ratio of the ice prisms, and because no exact solution is available that can presently be used for single-scattering by hexagonal prisms of arbitrary size, there are some combinations of wavelength and size for which we are unable to perform comparisons.

2. Formulation

[8] Following GW99, we represent a particle of volume V and surface area A by a collection of spheres. Since the ratio V/A for a sphere equals $r/3$, we define the radius of the equal-V/A sphere to be

$$r_{VA} = 3\frac{V}{A} \tag{1}$$

The number of equivalent spheres, n_s, relative to the number of nonspherical particles, n, is given by

$$\frac{n_s}{n} = \frac{3V}{4\pi r_{VA}^3}. \tag{2}$$

[9] These formulae can be readily applied to the case of hexagonal prisms. Figure 1 shows three representative cases with different aspect ratios, each characterized by dimensions a and c specifying the half-width of the basal face (a-axis dimension) and the length (c-axis dimension) respectively. The radii of the equal-V/A spheres are then given by:

$$r_{VA} = \frac{3\sqrt{3}ac}{4c + 2\sqrt{3}a} \tag{3}$$

The number of spheres needed to represent one prism is then determined from equations (2) and (3) using

$$V = \frac{3\sqrt{3}a^2c}{2} \tag{4}$$

It is convenient to define the aspect ratio, Γ, for hexagonal prisms as follows:

$$\Gamma \equiv \frac{c}{2a} \tag{5}$$

Equations (1)–(5) can be combined to give

$$r_{VA} = \frac{3\sqrt{3}a\Gamma}{4\Gamma + \sqrt{3}} \tag{6a}$$

$$\frac{n_s}{n} = \frac{\left(4\Gamma + \sqrt{3}\right)^3}{36\pi\Gamma^2} \tag{6b}$$

and

$$V = 3\sqrt{3}\, a^3\, \Gamma. \tag{6c}$$

[10] Equation (6b) shows that the number of spheres per crystal depends only on the aspect ratio. Included in Figure 1 are the values 3.6, 1.7, and 3.6 of n_s/n for aspect ratios of 0.2, 1, and 5, respectively. For long columns with very large aspect ratios (Shimizu crystals, see Figure 1b of GW99) we find the following asymptotic value for r_{VA}:

$$r_{VA} = \frac{3\sqrt{3}a}{4} = 1.299a \tag{7a}$$

and

$$\frac{n_s}{n} = \frac{16\Gamma}{9\pi} = 0.5659\Gamma \tag{7b}$$

So n_s/n increases in proportion to Γ. For broad plates with very small aspect ratios we find

$$r_{VA} = \frac{3\,c}{2} \tag{8a}$$

and

$$\frac{n_s}{n} = \frac{\sqrt{3}}{12\pi\Gamma^2} \tag{8b}$$

In this case, r_{VA} is proportional to c while n_s/n is proportional to Γ^{-2}.

[11] The general dependence of $\frac{n_s}{n}$ versus Γ is shown in Figure 2. The number of spheres per prism goes through a minimum value of 1.65 for $\Gamma = 0.866$, and it reaches the asymptotic limits at aspect ratios below 0.02 and above 10. Equations (7a) and (8a) illustrate the principle that r_{VA} is determined mainly by the short dimension and that for long columns or thin plates the long dimension is used only for determining the number of spheres. A similar conclusion has been reached by *Mätzler* [2002] in a study of the correlation statistics of snow grains and their

implications for the optical and microwave properties for snowpacks.

3. Single Scattering

[12] The scattering properties of spheres were calculated from Mie theory [*Wiscombe*, 1979, 1980]. For collections of randomly oriented hexagonal crystals the following methods were applied: for particles that are large compared with the wavelength we used geometric optics [*Takano and Liou*, 1989; *Yang and Liou*, 1996a], and for small particles we used the finite difference time domain method, FDTD [*Yang and Liou*, 1995, 1996b]. For the geometric optics calculations we used the GOM2 code [e.g., *Takano and Liou*, 1989; *Yang and Liou*, 1996a; *Fu*, 1996] kindly provided by P. Yang and K.-N. Liou. For the FDTD calculations, P. Yang allowed us to use his program.

3.1. Geometric Optics Method

[13] The principles of the geometric optics method are asymptotic approximations of electromagnetic theory, valid for light-scattering computations involving particles with dimensions much larger than the incident wavelength [*Takano and Liou*, 1989]. This method has been used to evaluate single-scattering properties of cirrus clouds [*Fu*, 1996] and is useful for terrestrial snow packs. The method becomes more accurate as the size parameter increases. It is known to be accurate for typical sizes of cirrus crystals at solar wavelengths but is often inappropriate for thermal infrared wavelengths where the ice crystals are no longer large compared to the wavelength [*Fu et al.*, 1998].

[14] We performed computations for crystals as large as a few millimeters, to cover sizes found in surface snow as well as those found in clouds. Hexagonal plates have aspect ratios less than 0.5. At the extreme of large aspect ratios, ''Shimizu'' crystals, shown in Figure 1b of *Grenfell and Warren* [1999], commonly have values of Γ near 50. The size parameter defined by *Yang et al.* [1997] for hexagonal prisms is

$$x = \frac{2\pi}{\lambda}\sqrt{\frac{ac}{2}}$$

or from (5):

$$x = \frac{2\pi a}{\lambda}\sqrt{\Gamma}. \tag{9}$$

GOM2 remains accurate to size parameters as low as 40. For extreme values of aspect ratio, however, a criterion based solely on x is inadequate because the small dimension, l, of the prism will have a linear size parameter $[2\pi l/\lambda]$ that is much smaller than 40. Thus to ensure validity of GOM2, we performed the calculations only if all three of the following criteria were satisfied:

$$x \geq 40$$

$$\frac{2\pi a}{\lambda} \geq 40$$

$$\frac{\pi c}{\lambda} \geq 40. \tag{10}$$

3.2. Finite Difference Time Domain Method

[15] An accurate method for calculating the scattering of light by hexagonal ice crystals has been developed [*Yang and Liou*, 1995; *Sun et al.*, 1999] which has been used for size parameters up to about 15. This method generates a numerical solution of Maxwell's equations expressed as a coupled set of finite difference equations to calculate the electromagnetic field in the near field of a crystal. The far-field scattering matrix is generated using an appropriate volume integral over the electromagnetic field within the particle [*Yang and Liou*, 1996b]. Because the grid spacing must be chosen to be a fraction of the wavelength of the radiation, the number of nodes increases sharply with particle size, and the resulting computational load becomes correspondingly heavy. For small size parameters it was necessary to chose a somewhat finer grid spacing to resolve the exciting wave form accurately. Using the NCAR Blackforest supercomputer we were able to run calculations up to size parameters up to about 8 running for 6 hours using 10 processors at a time.

3.3. Results for Single Scattering

[16] The calculations yielded values for the extinction efficiency, Q_{ext}, the single scattering albedo, ω_o, and the phase function, $p(\Theta)$ or equivalently Q_{sca}, Q_{abs}, and the moments of the phase function, g_l. The first moment, g_1 is the asymmetry parameter, g. The spectral complex refractive index of ice used here is the same as was used in GW99.

[17] In order to average over the resonant peaks in the Mie phase functions, single-scattering results were combined over a log-normal distribution of particle sizes with a specified geometric mean radius, r_g, and a fixed geometric standard deviation, $\sigma_g = 1.23$ (cf. Figure 3 of GW99). For radiative flux calculations, the most useful single number to characterize a size distribution is the area-weighted mean radius, or ''effective radius,'' r_{eff} [*Hansen and Travis*, 1974]:

$$r_{eff} = \frac{\int r^3 n(r)dr}{\int r^2 n(r)dr}. \tag{11}$$

For a log-normal distribution [*Reist*, 1993], r_{eff} is given by

$$r_{eff} = r_g \exp\left[2.5\left(\ln \sigma_g\right)^2\right]. \tag{12}$$

For $\sigma_g = 1.23$, we obtain $r_{\text{eff}} = 1.11\ r_g$. In practice, because the log-normal distribution was truncated at the wings, a numerically-determined conversion factor $r_{\text{eff}} = 1.09\ r_g$ was found to be more accurate for the computations we show here. In the discussions throughout the rest of the paper, size distributions are identified by the value of r_g specified, unless otherwise indicated. Geometric optics single-scattering results were combined similarly, i.e., a log-normal distribution over the a-axis dimension for a given aspect ratio. Because of greater computational requirements, FDTD results were not averaged over size distributions. (*Grenfell and Warren* [1999] stated that their distributions used $\sigma_g = 1.6$, but in fact they used $\sigma_g = 1.23$. The conversion

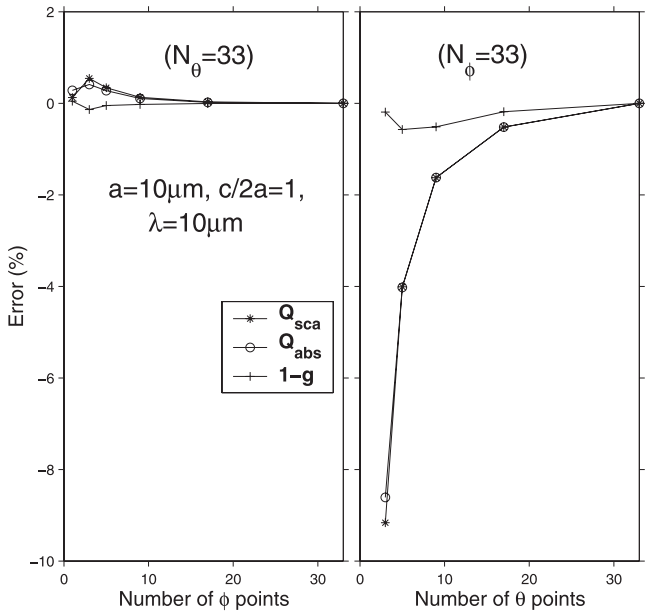

Figure 3. Discretization error in FDTD for calculations of Q_{sca}, Q_{abs}, and (1-g) for an assembly of randomly oriented columns with a = 10 μm, $\Gamma = c/2a = 1$, λ = 10 μm, versus the number of φ and θ orientations sampled, N_ψ and N_θ, respectively. The solution is assumed to be accurate for N_θ = 33 and N_φ = 33.

from r_g to r_{eff} given in the caption to their Figure 7 is therefore incorrect; the correct conversion according to equation (12) is $r_{eff} = 1.11\ r_g$.)

[18] The phase functions were computed at an angular sampling density selected so that 10 to 20 points were used for scattering angles from 0° to 1°, with resolution coarsening to 1° for larger scattering angles. Phase functions were numerically integrated to obtain moments (g_l) for use in multiple-scattering calculations. The numerical quadrature consisted of a trapezoidal rule with respect to cos(Θ) in which the logarithm of the phase function was interpolated using a spline algorithm.

[19] Because the computer time required for the FDTD calculations was substantial, it was important to optimize the number of discrete particle orientations needed for an accurate solution. We investigated the accuracy of the calculation of Q_{sca}, Q_{abs}, and (1-g) versus the number of discrete polar (θ) and azimuthal (ϕ) orientations assuming that the solution is accurate for n_φ = 33 and n_θ = 33. Results are shown in Figure 3 for prisms with a = 10 μm and Γ = 1 at a wavelength of 10 μm. They indicate an error of approximately 0.1% in all three variables for n_φ = 8 and n_θ = 33, while for n_φ = 33 and n_θ = 17 the error is about 0.3% in Q_{sca} and Q_{abs} and about 0.1% in (1-g). Errors are relatively insensitive to n_φ but they increase rapidly as n_θ decreases below about 10. We anticipate that this threshold will increase for significantly larger particles. For the results shown in this paper we used n_φ = 11 and n_θ = 10.

[20] Results of the single-scattering calculations for randomly oriented prisms are shown in Figures 4, 5, and 6for aspect ratios of 0.2 (plates), 1 (equidimensional crystals), and 5 (columns) respectively. In each figure, values of Q_{ext}, 1-ω_o, and g are plotted versus wavelength for a values of 1, 5, 10, 20, and 100 μm. The crosses indicate the FDTD results and the broad lines show the GOM2 values, each covering their respective wavelength domains. For GOM2 the range of applicability is specified by equation (10). This is why no GOM results are shown for a = 1 μm. For FDTD we were limited by the available computer capabilities and the number of cases is therefore more sparse. The narrow solid lines show the results for the equivalent spheres. The wavelength range studied (0.2–25 μm) covers essentially the entire solar shortwave and terrestrial longwave spectral regions.

[21] The extinction efficiency and single-scattering coalbedo of the cylinders are closely approximated at all wavelengths by the values for the corresponding equal-V/A spheres. For Γ = 0.2 and 5, the asymmetry factor is also closely represented by the equivalent spheres; however, this is not true for other values of Γ. For example, when Γ = 1 (Figure 5), (1-g) for the spheres is only half that of the prisms for wavelengths less than about 3 μm. As pointed out by *Liou and Takano* [1994] and GW99, among others, the difficulty with an equivalent sphere representation is in matching the angular distribution of the single scattering. Irradiance calculations are sensitive to the value of g unless the medium is strongly absorbing. As is evident in Figure 5, the largest departures of g from the true values arise for larger particles and at visible wavelengths, where the particles are most transparent.

[22] To investigate how well g values for the equivalent spheres represent the actual values for the hexagonal prisms, we show in Figure 7 the dependence of g on aspect ratio for r_{VA} = 50 μm and λ = 0.5 μm. The hexagonal prisms shown in the figure for Γ = 0.2, 1, and 5 are drawn accurately to scale. We see that the agreement in g occurs at aspect ratios of approximately 0.2 and 14, and the greatest departure corresponds to Γ = 1 where the asymmetry parameter for the spheres is too large. Thus we expect significant errors in irradiance for equidimensional crystals and very thin plates, but for very long columns the equivalent spheres may produce accurate results. In a real cloud which contains a distribution of aspect ratios, the errors will be smaller than for the extreme case of the equidimensional crystal. *Walden et al.* [2003, Figure 4a] measured the c-axis and a-axis lengths of 4000 hexagonal prisms at the South Pole, and found a distribution of aspect ratios; most were between 0.2 and 20.

[23] This behavior of g is most prominent for large size parameters where GOM2 is applicable. It is due to a combination of two effects. The presence of sharp edges and planes intersecting at right angles in the hexagonal prisms tends to enhance side and backscattering relative to spheres [*Liou*, 1973, Figure 1; *Wendling et al.*, 1979, Figure 8; *Mishchenko et al.*, 1996, Figure 1]. This acts to reduce the value of g. In contrast, rays passing through parallel faces of plates are scattered directly forward (“delta-transmission”) and tend to increase g relative to the equivalent spheres because delta-transmission does not occur for spheres. The former effect is dominant for equidimensional crystals where the smallest fraction of incident rays are undeflected, so as Γ departs from unity, g increases to asymptotic values above those of the equivalent sphere. These limits are about 0.90 and 0.96 for large and small Γ values, respectively.

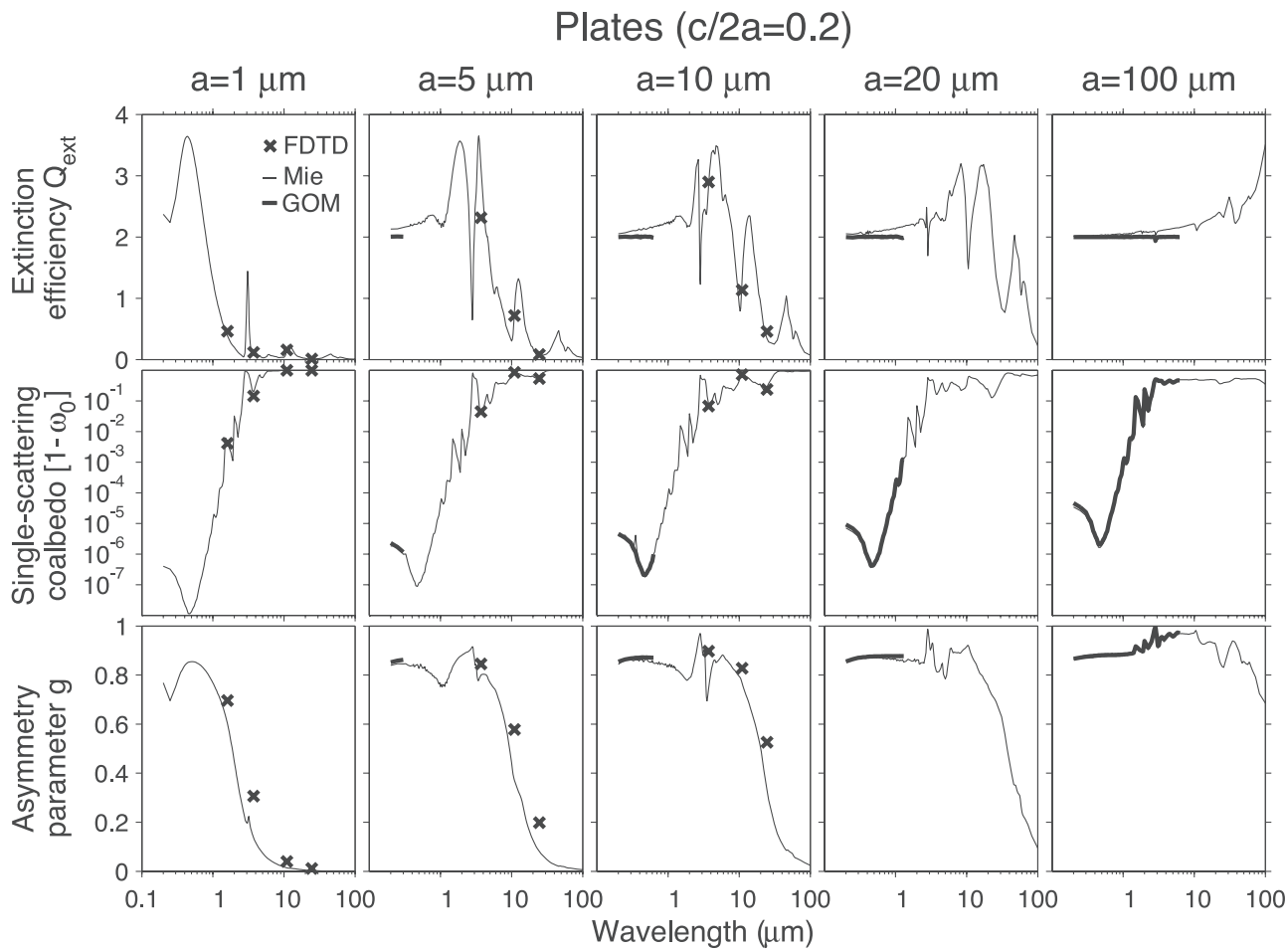

Figure 4. Extinction efficiency (Q_{ext}), single scattering coalbedo (1-ω_o), and asymmetry parameter (g) versus wavelength for randomly oriented hexagonal ice plates with $c/2a$ = 0.2 and the corresponding equal-V/A spheres. The geometric mean values of a for the distributions of hexagonal prisms are indicated at the top of each column. The crosses show the results of FDTD calculations, the thick solid lines show the GOM2 results, and the thin lines are for the equivalent spheres.

[24] Errors in single scattering do not necessarily propagate to errors in multiple scattering. For example, Figures 4 and 6 show significant errors in g for λ = 11 and 24.6 μm; but because (1-ω_o) is so large at these wavelengths, an ice cloud is almost totally absorbing, and errors in g have little effect on computations of radiative fluxes.

4. Multiple Scattering

[25] We now compare the bulk radiative properties of a horizontally homogeneous cloud of randomly oriented hexagonal ice columns to those of a cloud of equal-V/A spheres. Calculations of the apparent optical properties (hemispherical reflectance, absorptance, and transmittance) were carried out for a cloud consisting only of ice crystals, for selected wavelengths in the range 0.5–24.6 μm using a four-stream delta-M discrete-ordinates program [*Grenfell*, 1991]. To isolate the optical properties of the cloud itself, the model consisted of a single homogeneous plane parallel cloud layer over a black surface at 0°K illuminated from above by a plane wave at a zenith angle of 60°. In the thermal infrared, the absorptance can be equated to the directional emissivity at an emission angle of 60°. We plot the apparent optical properties as functions of the ice water path (IWP), defined as the total mass per unit area, integrated vertically through the cloud. The relation of IWP to cloud optical depth, τ, is given by equation (13) (equation (11) of GW99):

$$\tau = \frac{A_p}{V}\frac{Q_{ext}}{\rho_{ice}} IWP, \tag{13}$$

where A_p is the projected area, averaged over orientation, of a single particle (sphere or prism) and ρ_{ice} is the density of pure ice, 917 kg/m^3. For convex particles in general and hexagonal prisms in particular, $A_p = A/4$ [*Vouk*, 1948]; thus

$$\tau = \frac{A}{4V}\frac{IWP \cdot Q_{ext}}{\rho_{ice}}. \tag{14}$$

In terms of the radius of the equivalent sphere, we have from equation (1):

$$\tau_p = \frac{3}{4r_{VA}}\frac{IWP \cdot Q_{ext}(p)}{\rho_{ice}}, \tag{15}$$

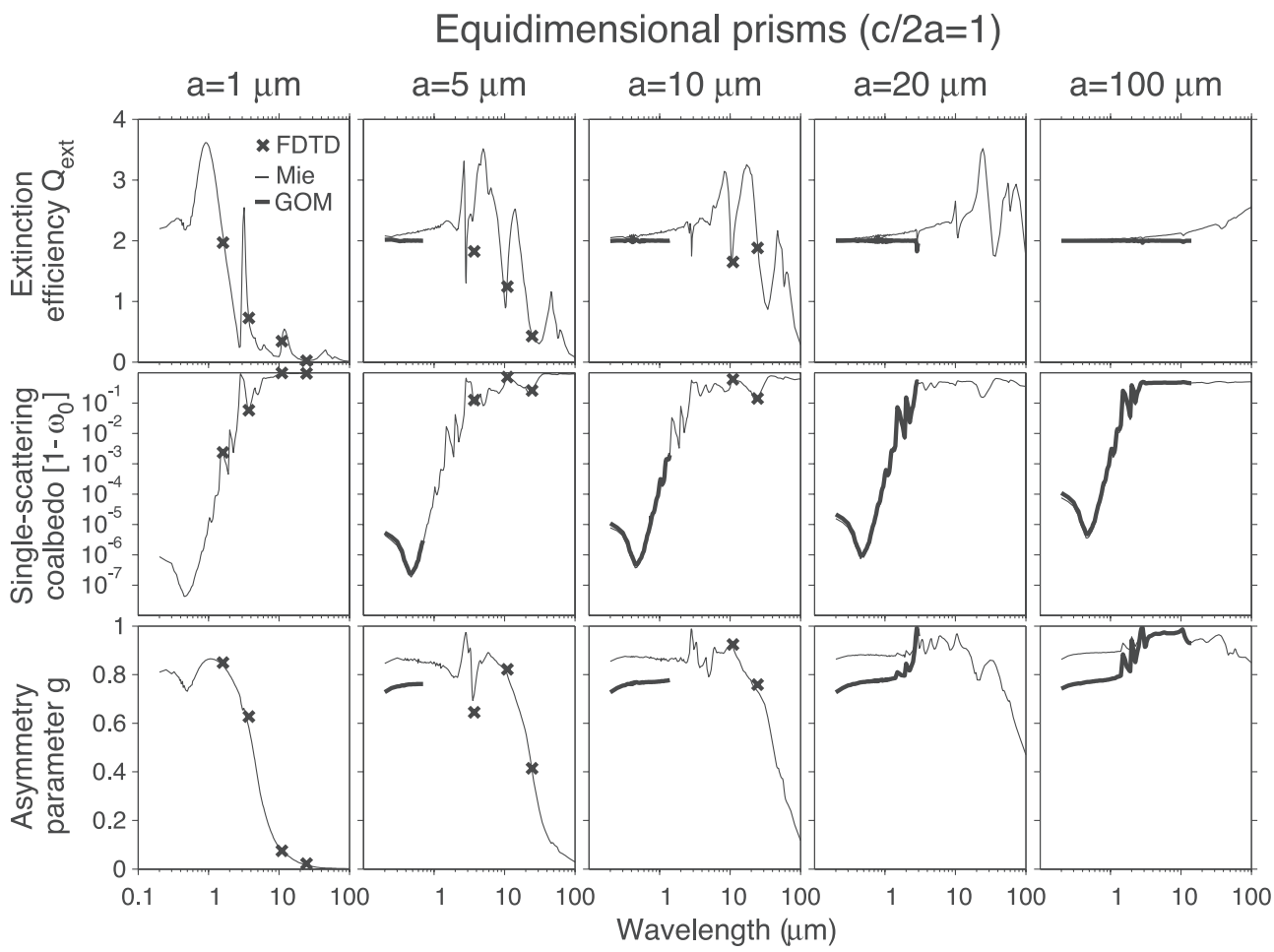

Figure 5. The same results as Figure 4 but for equidimensional crystals ($c/2a = 1$).

where the index p denotes prism. Since equation (14) also holds for the equivalent spheres, we obtain

$$\frac{\tau_{sph}}{\tau_p} = \frac{Q_{ext}(sph)}{Q_{ext}(p)}. \tag{16}$$

Note that this relationship is not limited to hexagonal prisms; it is exact for any convex particle.

[26] The input to the radiative transfer calculations are the single-scattering quantities for given a and Γ, as shown in Figures 4–6 for selected values of a, and τ, which is obtained from equations (15) and (6a) given *IWP*, a, and Γ. Calculations were carried out for ice-water-paths of 0.4 to 200,000 g m^{-2}, effective a-axis lengths of 0.5 to 200 μm, and aspect ratios 0.2, 1.0, and 5.0.

[27] Contours of approximate optical depths implied by all combinations of *IWP* and r_{VA} are shown in Figure 8. The precise optical depth depends on wavelength, because Q_{ext} depends on wavelength. For simplicity in Figure 8 we have simply used the geometric optics limit, $Q_{ext} = 2$, to plot the "geometric-optics" optical depth, τ_g. The ice-water paths and particle radii appropriate for snow, cirrus clouds, and polar stratospheric clouds are indicated in the figure.

[28] Figures 9 through 17 show the values of cloud reflectance, absorptance, and transmittance together with the differences between the exact solution and the equivalent-sphere results for the particular wavelengths 0.5, 1.6, 3.73, 11, and 24.6 μm. Reflectance is defined as the ratio of upwelling irradiance above the cloud to the incident irradiance. Absorptance and transmittance are ratios of absorbed and transmitted irradiance to incident irradiance. The minimum size parameters used for GOM2 results are as specified by equation (10). FDTD results were achievable only for size parameters up to about 8 owing to limitations in computing resources, resulting in a gap for intermediate particle sizes indicated in the figures by the shaded areas.

[29] The results shown in Figures 9–17 span a very large range in optical depth, from approximately 10^{-3} to 2×10^5, as shown in Figure 8, covering reflectance values of essentially zero for the smallest optical depths up to reflectance saturation with essentially zero transmittance for the largest optical depths. For large particles, reflectance decreases with increasing particle size, as seen in the upper left frame of Figure 9 for $\lambda = 0.5$ μm. For very small particles this trend reverses, as seen for a <1 μm at $\lambda = 1.6$ μm and $\lambda = 3.73$ μm. This is because in the geometric optics limit Q_{ext} is a constant ($Q_{ext} = 2$), so $\tau \sim r_{VA}^{-1}$ (equation (15)), whereas in the Rayleigh regime ($r \ll \lambda$), $Q_{ext} \sim r^4$ so $\tau \sim r_{VA}^3$.

[30] The errors in visible reflectance ($\lambda = 0.5$ μm in Figures 9, 12, 15) are greatest where the reflectance is near 0.5; the errors are small for very thin and very thick clouds.

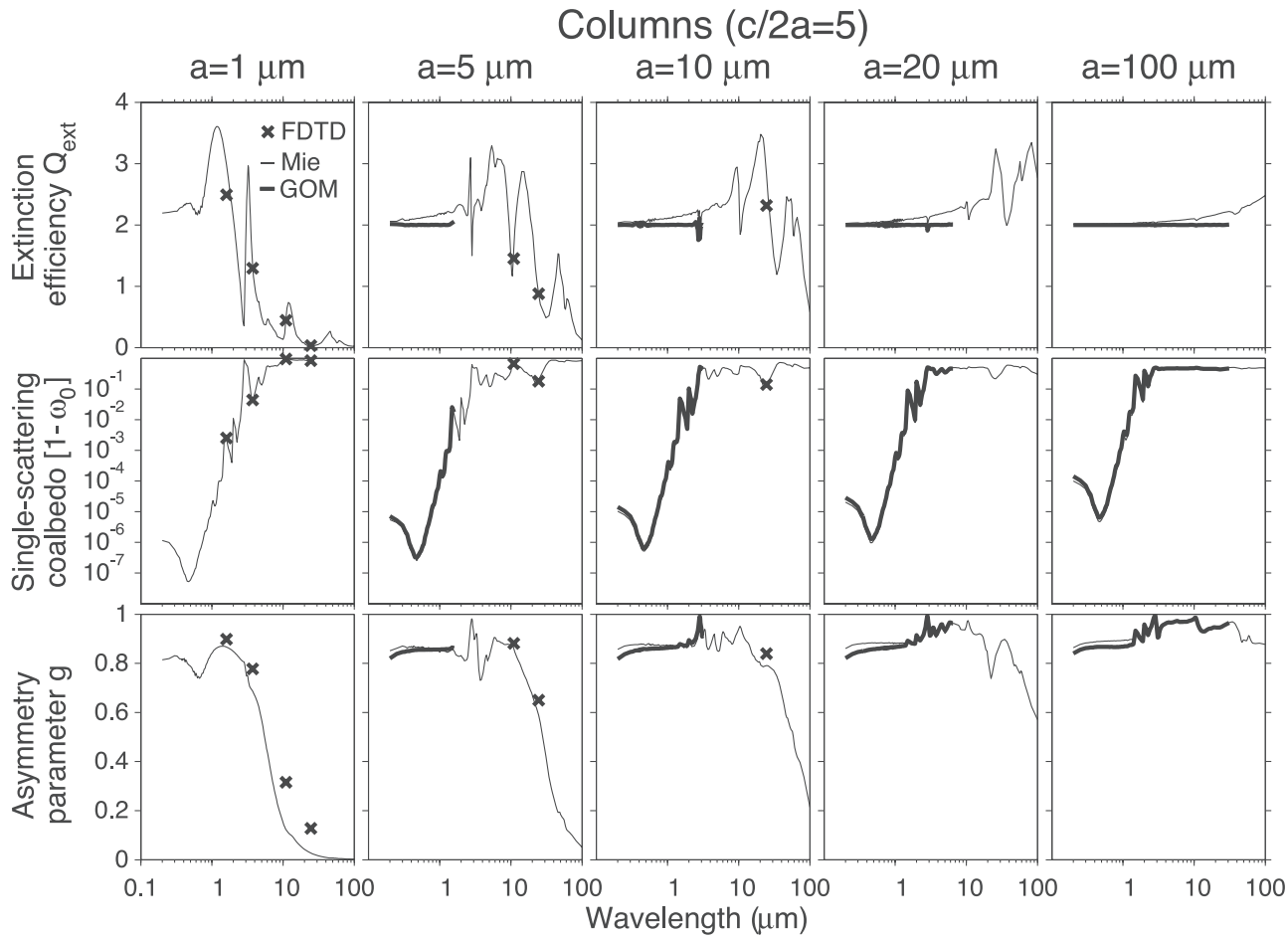

Figure 6. The same results as Figure 4 but for columns ($c/2a$ = 5).

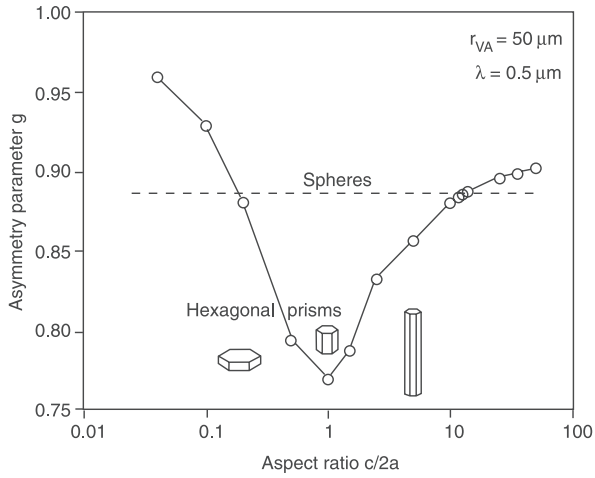

Figure 7. Asymmetry parameter versus aspect ratio for hexagonal prisms corresponding to equivalent spheres of 50 μm radius at a wavelength of 0.5 μm. The dashed line gives the g value for the equal-*V/A* spheres. The crystal shapes for aspect ratios 0.2, 1, and 5 are drawn to scale.

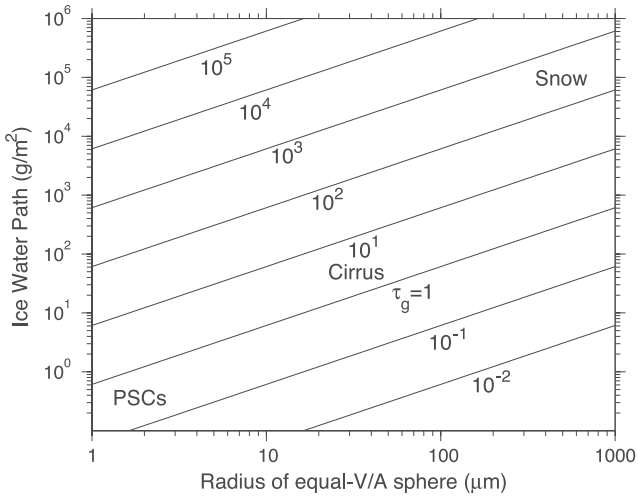

Figure 8. Contours of constant optical depth (τ_g) in the geometric-optics limit (Q_{ext} = 2) for the ranges of ice water path and radius of equal-*V/A* spheres covered in Figures 9–17. The combinations of ice water paths and particle radii appropriate for snow, cirrus clouds, and polar stratospheric clouds (PSCs) are indicated.

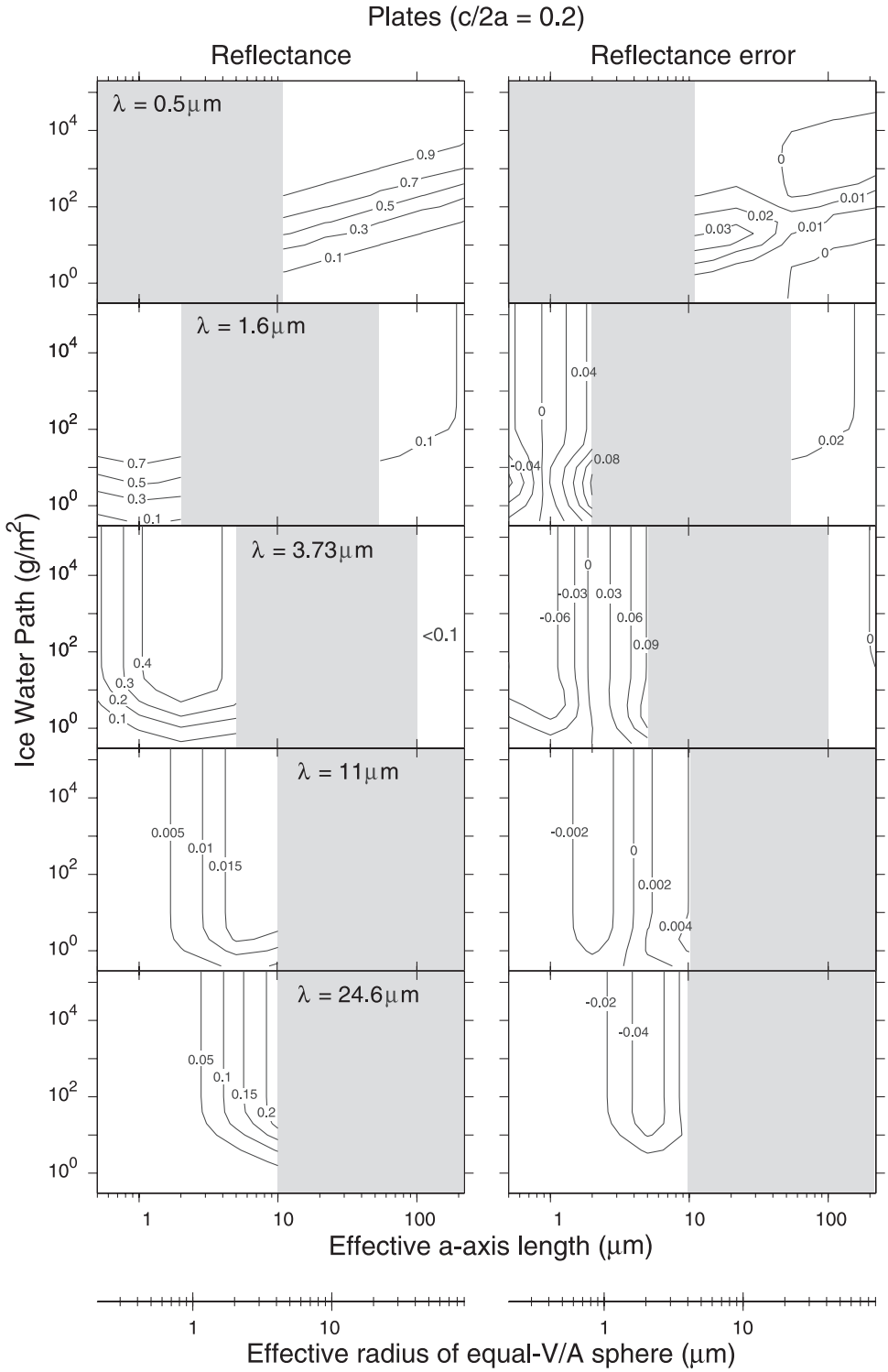

Figure 9. Contours of reflectance of clouds consisting of ice plates ($c/2a$ = 0.2) and of the corresponding errors introduced by the use of equal-*V/A* spheres to represent the plates, as functions of ice water path and *a*-axis length, for the five wavelengths (λ) specified. The corresponding radius (r_{eff}) of the equal-V/A spheres is also given as the lower abscissa. The plotted error is the approximate reflectance (using spheres) minus the true reflectance.

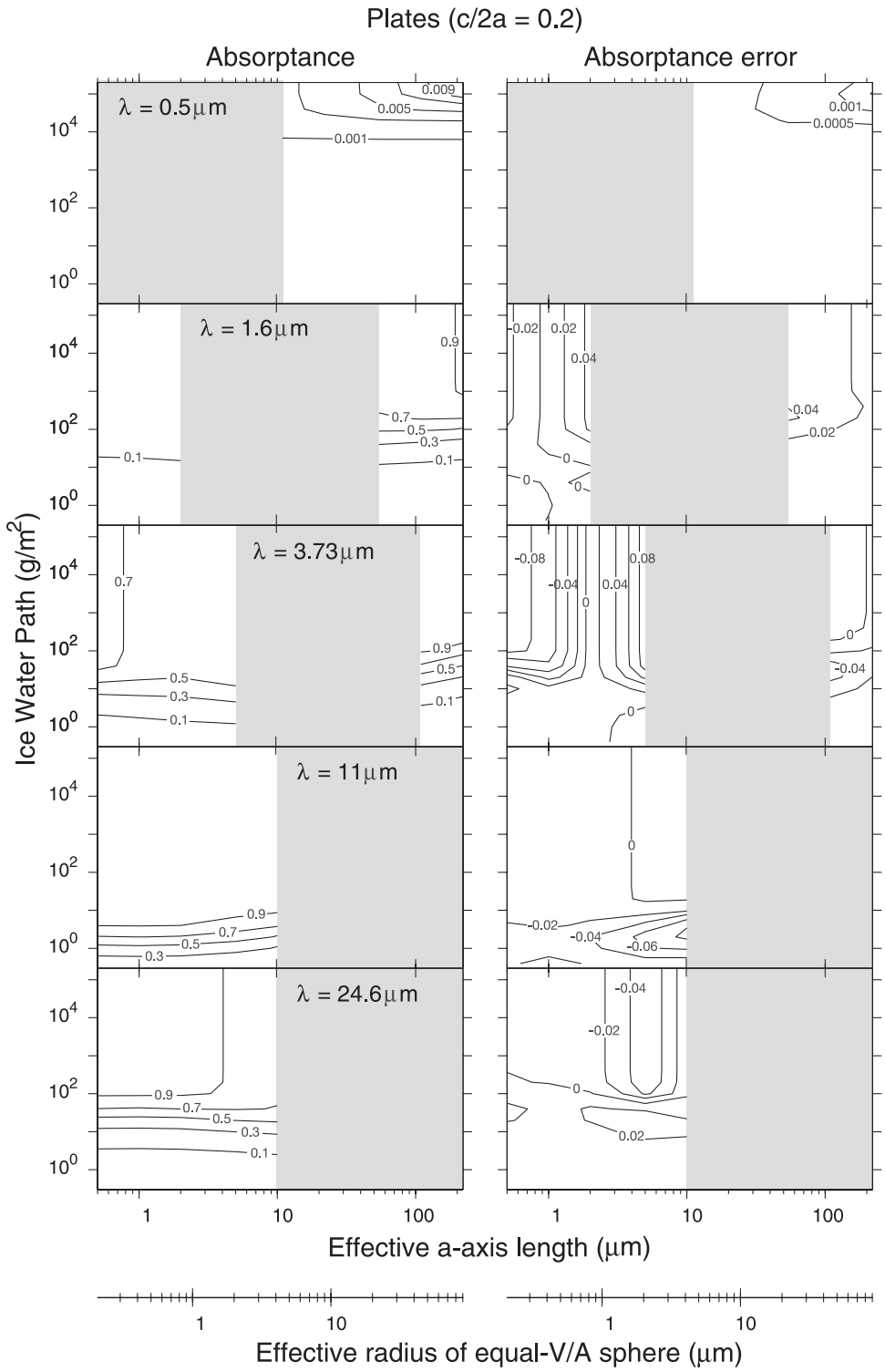

Figure 10. Same as Figure 9 but for absorptance.

The absorptance error is very small in the visible range because the absorptance itself is small, so the transmittance error is the same as the reflectance error with opposite sign.

[31] For the plates ($(c/2a) = \Gamma = 0.2$), the errors in all three quantities are less than 0.04 over most of the three-dimensional space of λ, a, and *IWP,* and less than 0.02 over much of that space, in particular for the large size parameter (GOM2) regime. The zones of vertical isolines indicate the regions of large τ where the reflectance is saturated. The magnitudes of the maximum errors are 0.09 for reflectance (λ = 3.73 μm), 0.08 for absorptance (λ = 3.73 μm), and 0.09 for transmittance (λ = 1.6 and 3.73 μm); these largest errors generally occur only for IWP values of about 1 to 10 g/m^2. They arise primarily from differences in total optical depth between the cloud of crystals and the cloud of

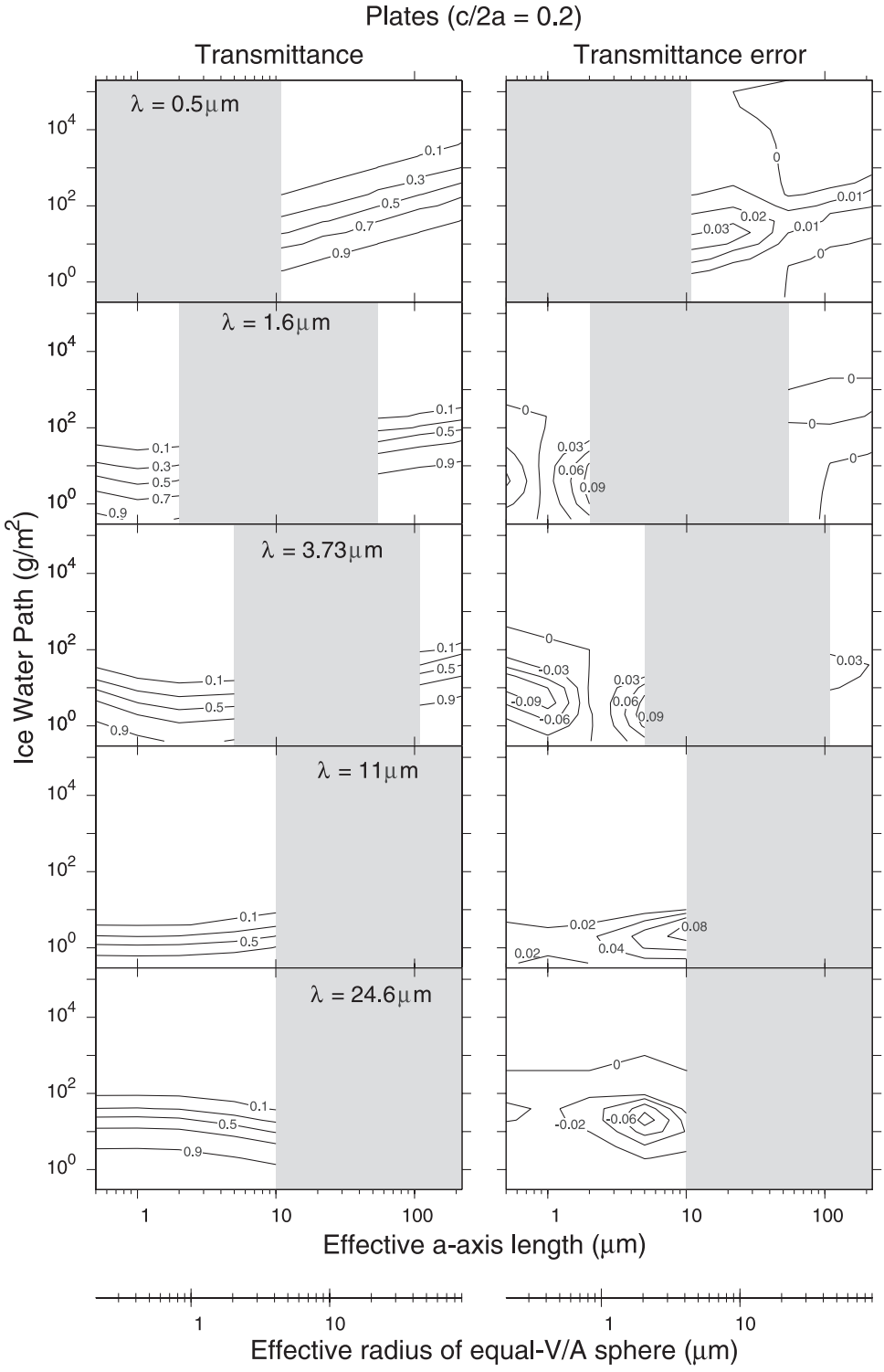

Figure 11. Same as Figure 9 but for transmittance.

spheres as a result of differences in Q_{ext} as indicated by equation (16). These differences occur for small size parameters, in the FDTD range, and for transmittances of about 0.5 where transmittance is most sensitive to changes in IWP. The same effect is apparent but to a lesser degree for the comparison with infinite cylinders [GW99] and the difference in Q_{ext} values is consistent with the results of *Fu et al.* [1999, Figure 3]. If we were to require arbitrarily that $\tau_p = \tau_{sph}$ this error would be reduced considerably, but the equivalent sphere representation would no longer be self-consistent.

[32] For equidimensional prisms (Figures 12–14), the magnitude of the errors is generally less than 0.06. At 24.6 μm the errors are as small as those for $\Gamma = 0.2$.

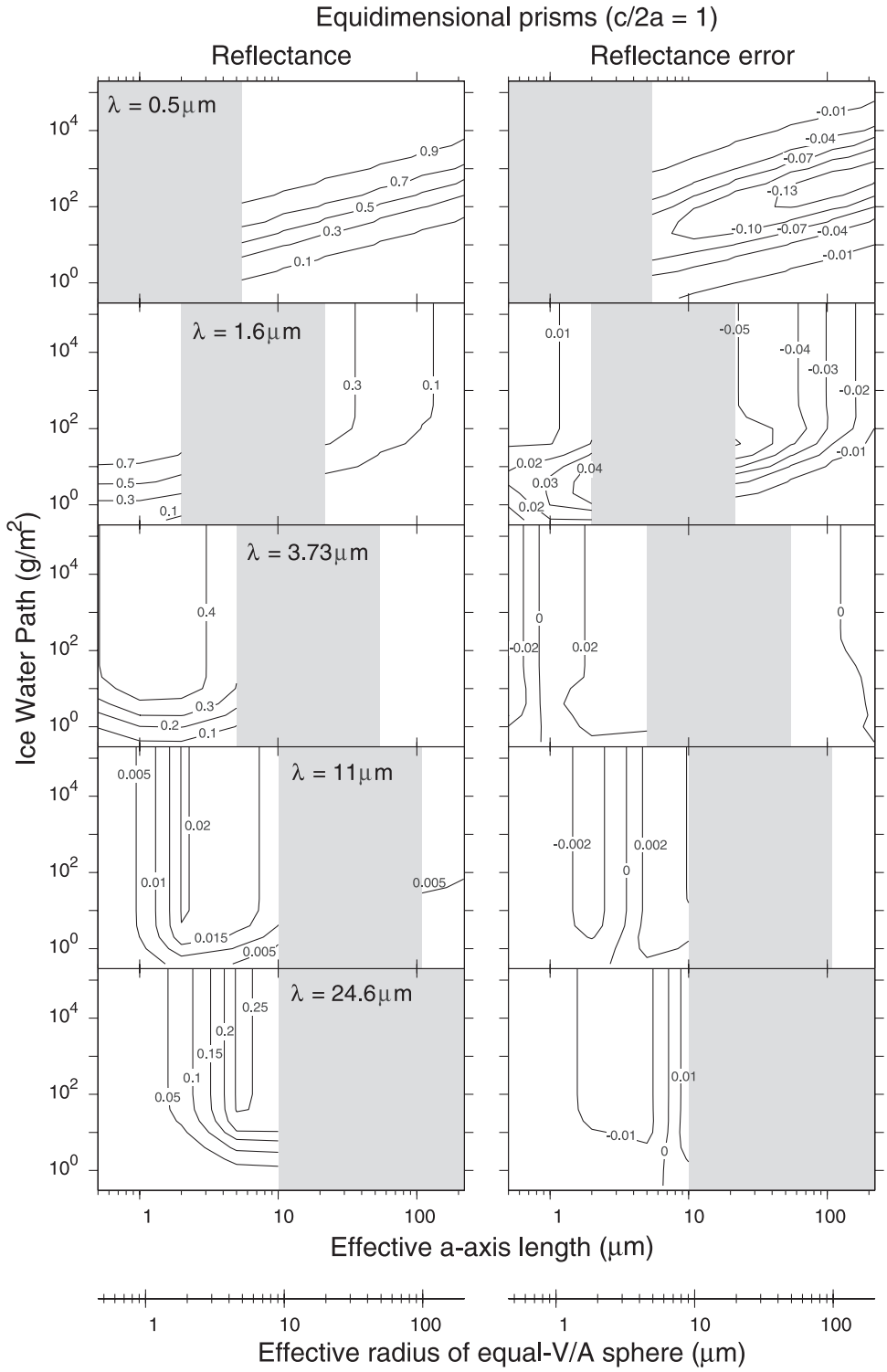

Figure 12. Reflectance and reflectance errors. Same as for Figure 9 but for equidimensional prisms ($c/2a = 1$).

There is, however, a significant error of as much as 0.13 for reflectance and transmittance at visible wavelengths because the asymmetry parameters calculated for the equivalent spheres are significantly larger than for the prisms. As is evident from Figure 7, the case of $\Gamma = 1$ shows the greatest difference between the prisms and the spheres, and the error decreases rapidly as Γ departs from unity.

[33] For columns, $\Gamma = 5$ (Figures 15–17), the situation is similar to the case $\Gamma = 0.2$. The asymmetry parameters of

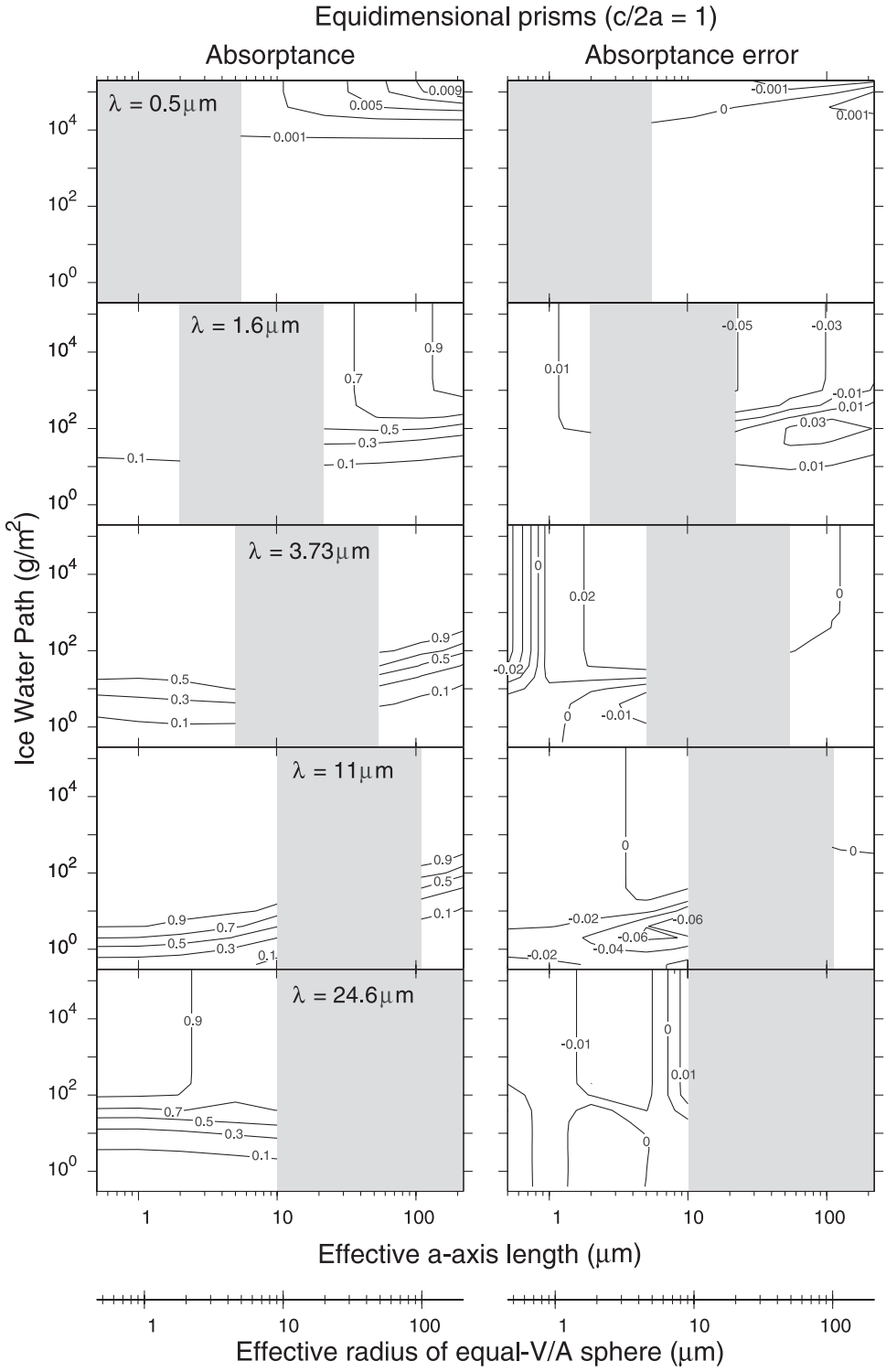

Figure 13. Same as for Figure 12 but for absorptance.

the columns are again close to those of the spheres. The maximum errors are generally less than 0.04 and occur where transmittance is most sensitive to changes in IWP.

[34] In all of these figures (Figures 9–17) there is a large blank region of intermediate crystal sizes where we were unable to compute radiative properties exactly because of the limitations of the FDTD method. In the future this region may become accessible as the FDTD method is made more efficient and computers become more powerful. In the meantime we can refer to GW99 as a guide to what errors will be caused by the equivalent-sphere representation in this size domain. The contours in Figures 7–9 of GW99 are rather flat across this size domain at wavelengths 0.5, 11, and 24.6 μm, but at λ = 1.6 and 3.73 μm they do show

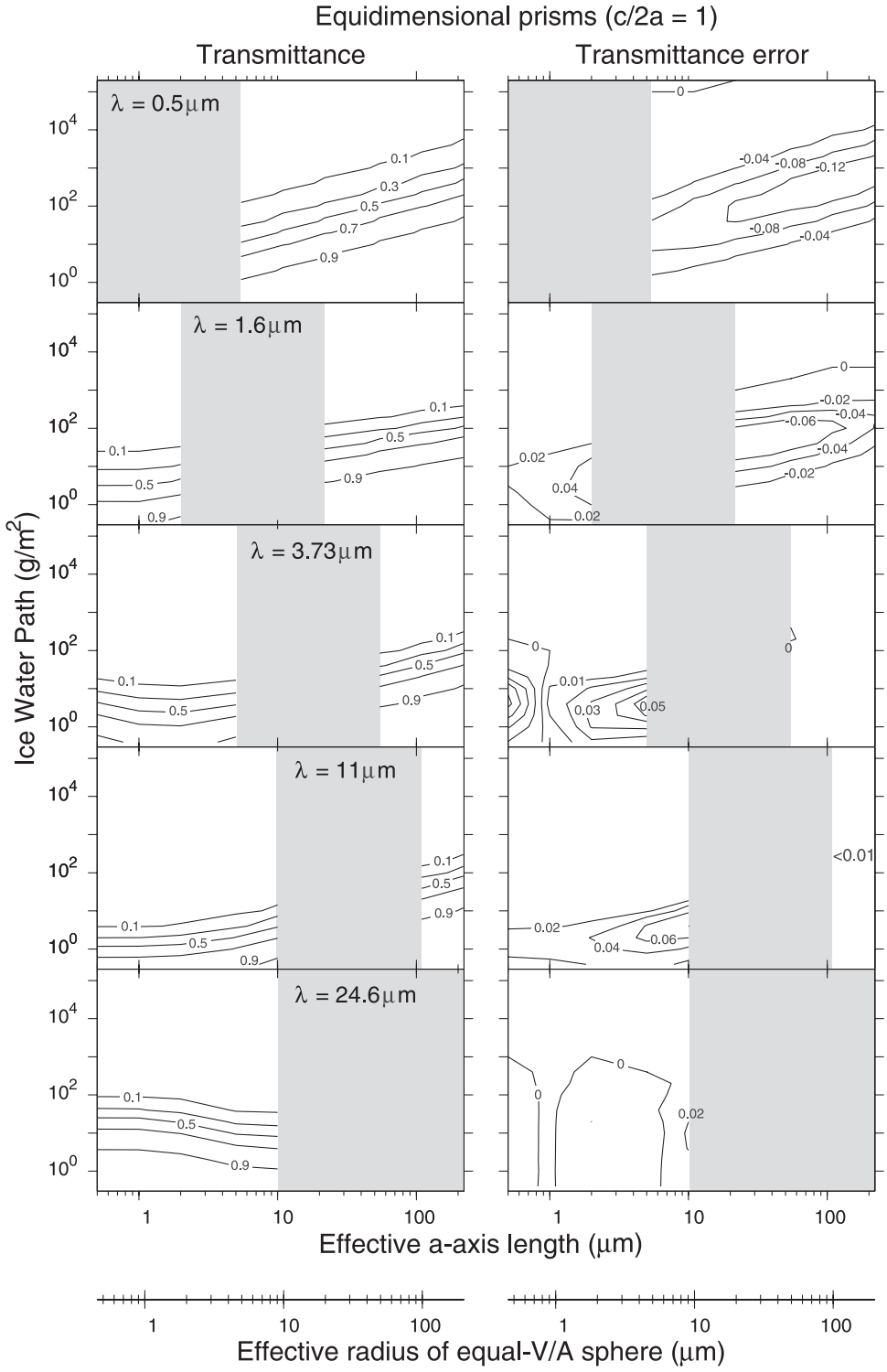

Figure 14. Same as for Figure 12 but for transmittance.

somewhat higher errors for intermediate sizes than for smaller and larger crystals.

5. Discussion and Conclusions

[35] The representation by equal-*V/A* spheres allows accurate computation of angular-averaged reflectance, transmittance, and absorptance for a multiple scattering medium consisting of columns with $\Gamma = 5$. Figure 7 indicates that the errors for any columns with $\Gamma > 5$ should be no larger than those shown for $\Gamma = 5$. For $\Gamma < 5$ the domain of validity is not universal. Errors are quite small over most of the parameter space (a, λ, Γ, IWP) accessible to FDTD and geometric-optics calculations but can exceed 0.1 for certain combinations of these parameters. In particular, for equidimensional prisms the use of equal-*V/A*

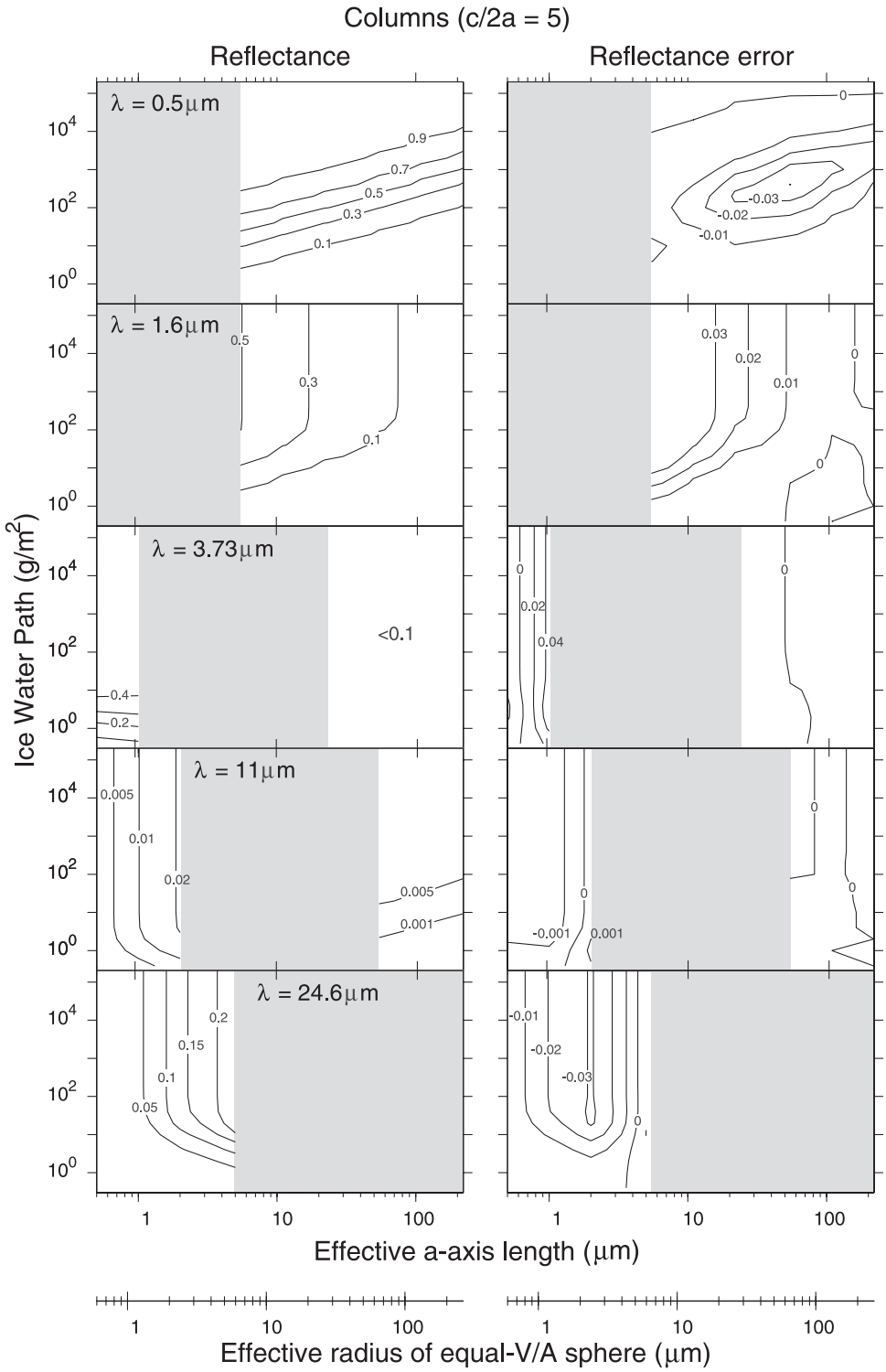

Figure 15. Reflectance and reflectance errors. Same as Figure 9 but for columns ($c/2a = 5$).

spheres causes a large underestimation of the visible reflectance for clouds of intermediate optical depth where reflectance ≈0.5. The practical significance of this error depends on the abundance of hexagonal prisms with $\Gamma < 5$ in real clouds.

[36] An analysis of atmospheric ice crystals collected at South Pole station during the winter [*Walden et al.*, 2003] shows that there is a gap at $\Gamma = 1$ where the occurrence of crystals is rare. The aspect ratios appear to have a bimodal distribution with median values of Γ of about 0.4 and 3. Figure 7 shows, however, that the error in g at $\lambda = 0.5$ μm is almost as large for $\Gamma = 0.4$ as for $\Gamma = 1$. The equal-*V/A* prescription will therefore overestimate the visible transmittance of Antarctic clouds.

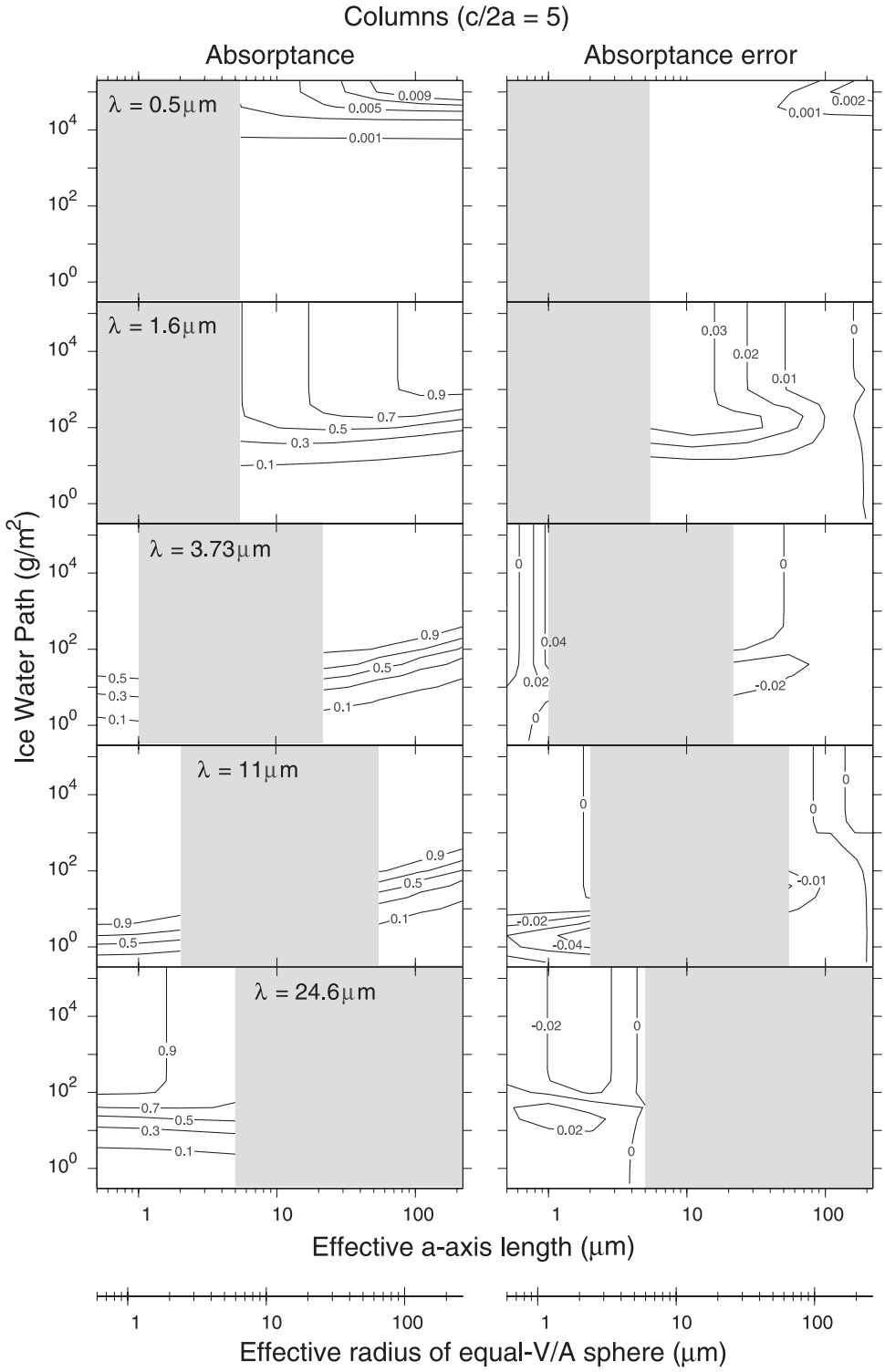

Figure 16. Same as for Figure 15 but for absorptance.

[37] The explanations given in the discussion of Figure 7 for the discrepancy between g and g_s depend on the pristine shapes of the crystals. Such crystals do exist in the Antarctic atmosphere [GW99, Figure 1; *Walden et al.*, 2003], but cirrus clouds, which occur worldwide, are of much greater climatic significance. In general their crystals are rarely of the pristine type considered here. They are made up of more irregular crystals, such as complex clusters of hollow bullets with nonparallel walls [*Ono*, 1969; *Heymsfield*, 1975; *Heymsfield and Platt*, 1984; *Lawson et al.*, 1998]. It will therefore be important to examine the ability of equal-*V/A* spheres to mimic the absorption and scattering by irregular

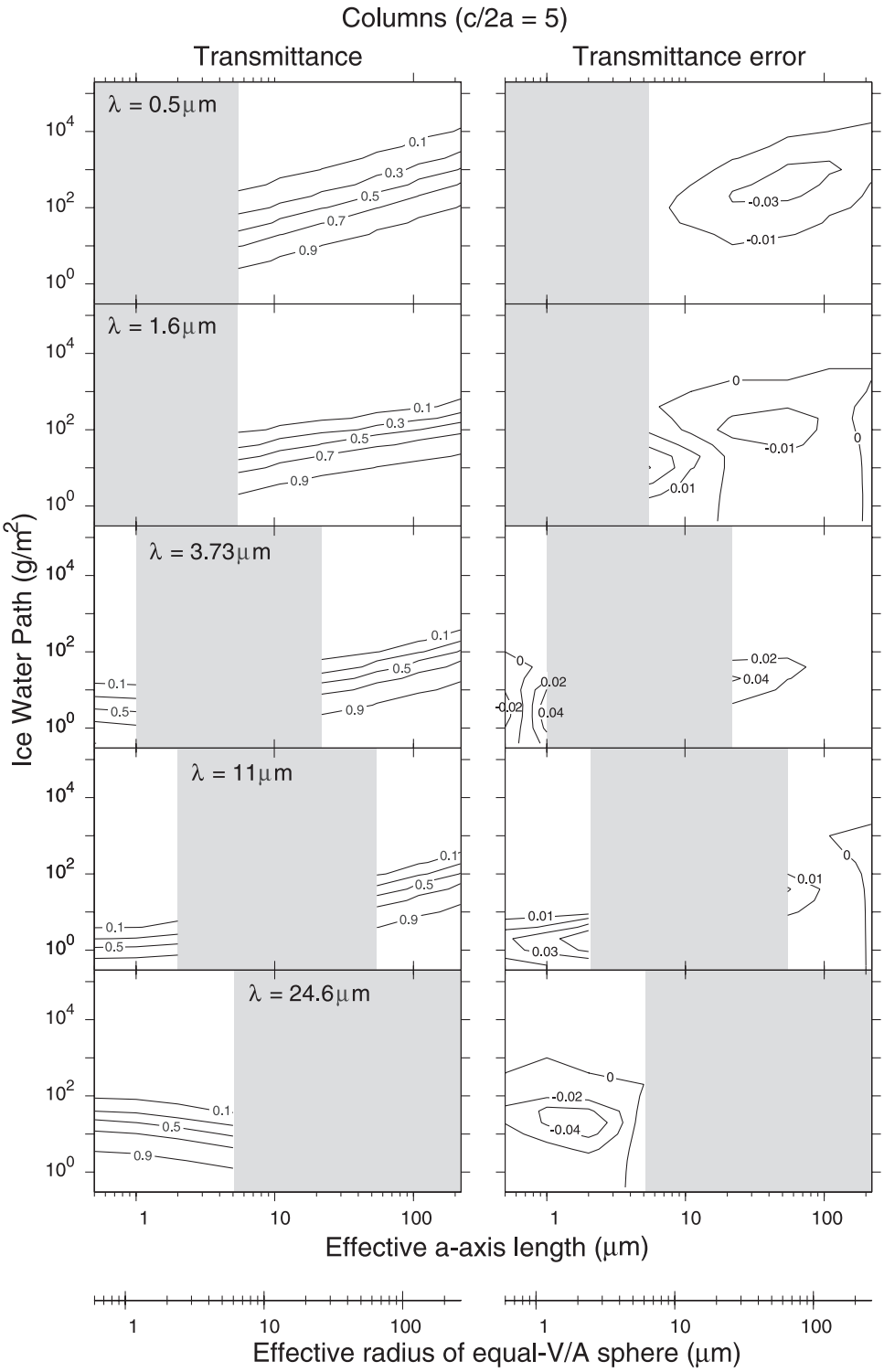

Figure 17. Same as for Figure 15 but for transmittance.

and hollow crystals. In that case, the value of V is the volume occupied by ice, and A is the total area of both internal and external surfaces.

[38] **Acknowledgments.** We are grateful to Wenbo Sun, Ping Yang, and Kuo-Nan Liou for making available their computer codes for randomly oriented hexagonal prisms and for generous assistance in making them run properly on our system. Tim Rahmes assisted with the initial single-scattering calculations. We thank Qiang Fu, Ping Yang, Kuo-Nan Liou, and Christian Mätzler for helpful discussions. We also thank the NCAR computing facility for providing resources on the Blackforest supercomputer. This research was supported by the National Science Foundation under grant OPP-98-13671.

References

Fu, Q., An accurate parameterization of the solar radiative properties of cirrus clouds for climate models, *J. Clim.*, *9*, 2058–2082, 1996.

Fu, Q., P. Yang, and W. B. Sun, An accurate parameterization of the infrared radiative properties of cirrus clouds for climate models, *J. Clim.*, *11*, 2223–2237, 1998.

Fu, Q., W. B. Sun, and P. Yang, Modeling of scattering and absorption by nonspherical cirrus ice particles at thermal infrared wavelengths, *J. Atmos. Sci.*, *56*, 2937–2947, 1999.

Grenfell, T. C., A radiative transfer model for sea ice with vertical structure variations, *J. Geophys. Res.*, *96*, 16,991–17,001, 1991.

Grenfell, T. C., and S. G. Warren, Representation of a nonspherical ice particle by a collection of independent spheres for scattering and absorption of radiation, *J. Geophys. Res.*, *104*, 31,697–31,709, 1999.

Hansen, J. E., and L. D. Travis, Light scattering in planetary atmospheres, *Space Sci. Rev.*, *16*, 527–610, 1974.

Heymsfield, A., Cirrus uncinus generating cells and the evolution of cirriform clouds, part I: aircraft observations of the growth of the ice phase, *J. Atmos. Sci.*, *32*, 799–808, 1975.

Heymsfield, A. J., and C. M. R. Platt, A parameterization of the particle size spectrum of ice clouds in terms of the ambient temperature and the ice water content, *J. Atmos. Sci.*, *41*, 846–855, 1984.

Lawson, R. P., A. J. Heymsfield, S. M. Aulenbach, and T. L. Jensen, Shapes, sizes and light scattering properties of ice crystals in cirrus and a persistent contrail during SUCCESS, *Geophys. Res. Lett.*, *25*, 1331–1334, 1998.

Liou, K.-N., Transfer of solar irradiance through cirrus cloud layers, *J. Geophys. Res.*, *78*, 1409–1418, 1973.

Liou, K.-N., and Y. Takano, Light scattering by nonspherical particles: remote sensing and climatic implications, *Atmos. Res.*, *31*, 271–298, 1994.

Mätzler, C., Relationships between grain size and correlation length of snow, *J. Glaciol.*, *48*, 461–466, 2002.

Mishchenko, M. I., W. B. Rossow, A. Macke, and A. A. Lacis, Sensitivity of cirrus cloud albedo, bidirectional reflectance and optical thickness retrieval accuracy to ice particle shape, *J. Geophys. Res.*, *101*, 16,973–16,985, 1996.

Ono, A., The shape and riming properties of ice crystals in natural clouds, *J. Atmos. Sci.*, *26*, 138–147, 1969.

Reist, P. C., *Aerosol Science and Technology*, McGraw-Hill, New York, 1993.

Sun, W., Q. Fu, and Z. Chen, Finite-difference time-domain solution of light scattering by dielectric particles with a perfectly matched layer absorbing boundary condition, *Appl. Opt.*, *38*, 3141–3151, 1999.

Takano, Y., and K. N. Liou, Solar radiative transfer in cirrus clouds, part I: Single scattering and optical properties of hexagonal ice crystals, *J. Atmos. Sci.*, *46*, 3–18, 1989.

Vouk, V., Projected area of convex bodies, *Nature*, *162*, 330–331, 1948.

Walden, V. P., S. G. Warren, and E. Tuttle, Atmospheric ice crystals over the Antarctic Plateau in winter, *J. Appl. Meteorol*, in press, 2003.

Wendling, P., R. Wendling, and H. K. Weickmann, Scattering of solar radiation by hexagonal ice crystals, *Appl. Opt.*, *18*, 2663–2671, 1979.

Wiscombe, W. J., Mie scattering calculations: Advances in technique and fast, vector-speed computer codes, *NCAR Tech. Note TN-140+STR [NTIS PB 301388]*, Natl. Cent. for Atmos. Res., Boulder, Colo., 1979.

Wiscombe, W. J., Improved Mie scattering algorithms, *Appl. Opt.*, *19*, 1505–1509, 1980.

Yang, P., and K. N. Liou, Light scattering by hexagonal ice crystals: Comparison of finite-difference time domain and geometric optics models, *J. Opt. Soc. Am.*, *12*, 162–176, 1995.

Yang, P., and K. N. Liou, Geometric-optics-integral-equation method for light scattering by nonspherical ice crystals, *Appl. Opt.*, *35*, 658–6568, 1996a.

Yang, P., and K. N. Liou, Finite-difference time domain method for light scattering by small ice crystals in three-dimensional space, *J. Opt. Soc. Am.*, *13*, 2072–2085, 1996b.

Yang, P., K. N. Liou, and W. P. Arnott, Extinction efficiency and single-scattering albedo for laboratory and natural cirrus clouds, *J. Geophys. Res.*, *102*, 21,825–21,835, 1997.

S. P Neshyba, Department of Chemistry, University of Puget Sound, 1500 N. Warner, Tacoma, WA 98416, USA. (nesh@ups.edu)

T. C. Grenfell and S. G. Warren, Department of Atmospheric Sciences, Box 351640, University of Washington, Seattle, WA 98195-1640, USA. (tcg@atmos.washington.edu; sgw@atmos.washington.edu)